

1                   **Plasma-catalytic removal of formaldehyde over Cu-Ce**  
2                   **catalysts in a dielectric barrier discharge reactor**

3       Xinbo Zhu<sup>a, b</sup>, Xiang Gao<sup>a, \*</sup>, Rui Qin<sup>a</sup>, Yuxuan Zeng<sup>b</sup>, Ruiyang Qu<sup>a</sup>, Chenghang Zheng<sup>a</sup>, Xin Tu<sup>b, \*</sup>

4

5       <sup>a</sup> State Key Laboratory of Clean Energy Utilization, Zhejiang University, Hangzhou, 310027, P. R.

6       China

7       <sup>b</sup> Department of Electrical Engineering and Electronics, University of Liverpool, Liverpool, L69

8       3GJ, UK

9

10      \*Corresponding authors:

11      **Dr. Xin Tu**

12      Department of Electrical Engineering and Electronics,

13      University of Liverpool,

14      Liverpool, L69 3GJ, UK

15      E-mail: [xin.tu@liv.ac.uk](mailto:xin.tu@liv.ac.uk)

16      Tel: +44-1517944513

17      **\* Prof. Xiang Gao**

18      State Key Laboratory of Clean Energy Utilization,

19      Zhejiang University,

20      Hangzhou 310027,

21      China

22      E-mail: [xgao1@zju.edu.cn](mailto:xgao1@zju.edu.cn)

23

24    **Abstract**

25    In this study, a coaxial dielectric barrier discharge (DBD) reactor has been used for plasma-catalytic  
26    removal of low concentration formaldehyde over a series of Cu-Ce oxide catalysts prepared by the  
27    citric acid sol-gel method. The effect of the Cu/Ce molar ratio on the removal of formaldehyde and  
28    CO<sub>2</sub> selectivity has been investigated as a function of specific energy density (SED). In comparison  
29    to the plasma-only process, the combination of plasma with the Cu-Ce binary oxide catalysts  
30    significantly enhances the reaction performance, while the presence of CuO or CeO<sub>2</sub> in the DBD  
31    reactor has a negative effect on the removal of HCHO. This suggests that the interactions between  
32    Cu and Ce species change the properties of the catalysts and consequently affect the performance of  
33    the plasma-catalytic process. The highest removal efficiency of 94.7% and CO<sub>2</sub> selectivity of 97.3%  
34    were achieved when the Cu<sub>1</sub>Ce<sub>1</sub> catalyst (Cu/Ce = 1:1) was placed in the DBD reactor at the SED of  
35    486 J L<sup>-1</sup>. The interaction between Cu and Ce species results in a larger specific surface area and pore  
36    volume, along with a greater formation of surface adsorbed oxygen (O<sub>ads</sub>), which favor the oxidation  
37    of formaldehyde in the plasma process. In addition, the redox cycles between Cu and Ce species  
38    facilitate the formation of additional active oxygen atoms and contribute to the plasma-catalytic  
39    oxidation reactions. Plausible reaction mechanisms involved in the plasma-catalytic oxidation of  
40    HCHO have been proposed.

41    **Keywords:** Plasma-catalysis; Dielectric barrier discharge (DBD); Formaldehyde; Cu-Ce catalysts

42

43

44

45

46 **Highlight**

47 • Cu-Ce binary catalysts show excellent HCHO removal efficiency and CO<sub>2</sub> selectivity.

48 • Electronic excitations become more important with increasing specific energy density.

49 • Surface adsorbed oxygen plays an important role in plasma-catalytic reactions.

50 • Both gas phase and surface reactions contribute to HCHO removal.

51

52

53

54

55

56

57

58

59

60

61

62

63

64

65

66

67

68    **1. Introduction**

69       Formaldehyde (HCHO) is a hazardous air pollutant that is mainly emitted from industrial  
70    processes such as the manufacturing of wood products and building materials, and combustion  
71    processes. As one of the toxic volatile organic compounds (VOCs), the emission of formaldehyde has  
72    become a great concern in our society due to its harmful effects on our health and environment,  
73    especially as a suspected carcinogen. Significant efforts have been devoted to the development and  
74    investigation of various pollution remediation technologies including adsorption, membrane  
75    separation, biological process, thermal combustion and catalytic oxidation for the removal of  
76    formaldehyde. However, conventional technologies are not cost-effective for the removal of low  
77    concentration VOCs (e.g. formaldehyde) in high volume waste gas streams. For example, thermal  
78    processes require large amounts of energy for heating the high volume gas flow to clean only a low  
79    concentration of environmental pollutants.

80       Non-thermal plasma (NTP) has been regarded as a promising method for the removal of a wide  
81    range of low concentration volatile organic compounds (VOCs) due to its non-equilibrium character,  
82    fast reaction, low energy cost and unique ability to initiate both physical and chemical reactions at  
83    low temperatures [1]. Energetic electrons generated in non-thermal plasma can collide with carrier  
84    gases, forming highly reactive species such as free radicals and excited atoms, molecules and ions.  
85    These species are capable of breaking most chemical bonds or initiating chemical reactions, leading  
86    to the removal of various VOC pollutants [2]-[5]. However, the selectivity toward the desired final  
87    products (e.g. CO<sub>2</sub> and H<sub>2</sub>O) through deep oxidation is typically low when using plasma discharge  
88    alone, whilst the formation of unwanted by-products is inevitable [3][5]. Recently, a hybrid plasma-  
89    catalysis technology has been developed to combine the advantages of high selectivity from catalysis

90 with the low temperature, fast reaction provided by non-thermal plasma [6]-[8]. The integration of  
91 plasma and catalysis has great potential to reduce the operating temperature of catalyst activation,  
92 enhance the removal efficiency of the gas pollutant and increase the selectivity of the desired final  
93 products to minimise the formation of unwanted by-products (such as NO<sub>x</sub>); all of which contribute  
94 to enhancing the energy efficiency of the process [8]-[10].

95       Catalysts are regarded as one of the most important factors to determine the reaction performance  
96 of a plasma-catalysis system. Different catalysts including  $\gamma$ -Al<sub>2</sub>O<sub>3</sub>, TiO<sub>2</sub>, zeolite 13X and NaNO<sub>2</sub>  
97 coated raschig rings, have been shown to enhance the process performance for the plasma-catalytic  
98 oxidation of formaldehyde [11][12]. Ding et al. found that the presence of Ag/CeO<sub>2</sub> catalysts in a  
99 dielectric barrier discharge (DBD) significantly improved the removal efficiency and CO<sub>2</sub> selectivity  
100 of formaldehyde, which can be attributed to the formation of plasma-enhanced catalytic redox cycles  
101 between Ag and Ce species [13]. Zhao et al. also reported a similar interaction effect from Ag and Cu  
102 in the AgCu/HZSM-5 for formaldehyde removal in a cycled storage–discharge (CSD) system [14].  
103 However, high costs of noble metals could limit the use of these catalysts for industrial applications.  
104 Up until now, the knowledge of supported metal oxide catalysts, especially the binary oxide catalysts,  
105 for the plasma-catalytic oxidation of formaldehyde is rather limited [15][16].

106       Cu-based catalysts have been widely used in the oxidation of VOCs due to their sufficient  
107 catalytic activity and relatively low cost [17]. Cerium oxide (CeO<sub>2</sub>) has been regarded as an effective  
108 promoter in thermal catalytic reactions due to its high oxygen storage capacities and redox properties  
109 between Ce<sup>4+</sup> and Ce<sup>3+</sup>. CeO<sub>2</sub> can also act as a local source/sink of oxygen species due to its high bulk  
110 oxygen mobility and oxygen vacancies [18]. Cu-Ce mixed oxides have been regarded as promising  
111 catalysts for thermal catalytic oxidation of VOCs, such as benzene and toluene, due to the strong

112 interactions between Cu and Ce species [19][20]. However, the combination of Cu-Ce oxide catalysts  
113 with non-thermal plasmas for the oxidation of VOCs has not yet been reported [21]. It is still not clear  
114 how the interactions between Cu and Ce species will affect the plasma-catalytic oxidation process.

115 In this study, a series of Cu-Ce oxide catalysts with different molar ratios have been prepared by  
116 a citric acid method. The effect of these catalysts on plasma-catalytic removal of formaldehyde as a  
117 function of specific energy density (SED) has been investigated in terms of formaldehyde removal  
118 efficiency and CO<sub>2</sub> selectivity. Catalyst characterization has been carried out using a wide range of  
119 analytic techniques such as Brunauer, Emmett and Teller (BET) surface measurement, X-ray  
120 diffraction (XRD) and X-ray photoelectron spectroscopy (XPS) to get a better understanding of the  
121 roles of these catalysts in the plasma-catalytic process. Plausible reaction mechanisms and pathways  
122 have also been proposed and discussed.

123

124 **2. Experimental Section**

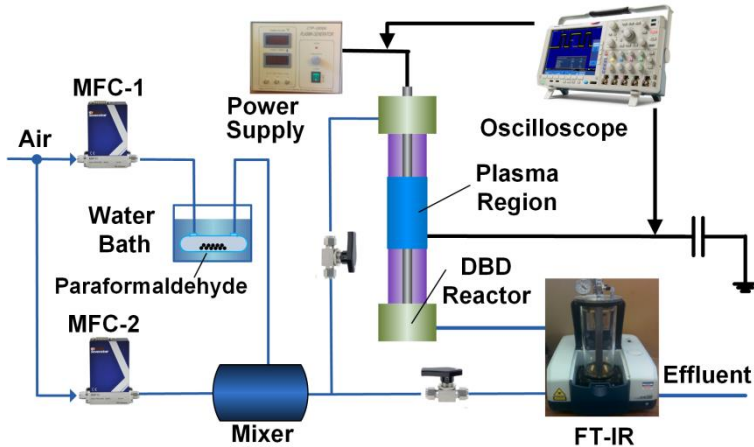
125 **2.1 Experimental Setup**

126 Fig. 1 shows the schematic diagram of the experimental setup. A 60 mm-long aluminum foil  
127 (ground electrode) was wrapped over a quartz tube with an inner diameter of 8 mm and wall thickness  
128 of 1 mm. A stainless steel rod with an outer diameter of 4 mm was placed in the axis of the quartz  
129 tube and acted as a high voltage electrode. As a result, the length of the discharge zone was 60 mm  
130 with a discharge gap of 2 mm. Catalysts (100 mg, 35-60 mesh) were packed in the discharge region  
131 and held by quartz wool, corresponding to a gas hourly space velocity (GHSV) of 600000 mL g<sup>-1</sup> h<sup>-1</sup>.

132 In this study, simulated dry air was used as carrier gas. Gaseous formaldehyde was acquired by  
133 feeding a dry air stream through paraformaldehyde powders (99.9%, Alfa Aesar) which were

134 contained in a vessel heated in a water bath (60 °C). The total flow rate for the experiments was fixed  
135 at 1 L min<sup>-1</sup> with a corresponding residence time of 0.23 s in the discharge area. The initial  
136 concentration of formaldehyde was kept at 57.7 ppm.

137



138

**Fig. 1.**

140

141 The DBD reactor was supplied by an AC high voltage power supply with a maximum peak  
142 voltage of 30 kV and a frequency of 10 kHz. A high voltage probe (Testec, HVP-15HF, 1000:1) was  
143 used to measure the applied voltage of the discharge, while a Tektronix P5100 probe was used to  
144 measure the voltage across the external capacitor C<sub>ext</sub> (0.47 μF). All the electrical signals were  
145 monitored by a digital oscilloscope (Tektronix 3034B). V-Q Lissajous method was used to calculate  
146 the discharge power (*P*) of the DBD reactor. In the present work, specific energy density has been  
147 defined as energy dissipated to the plasma per unit volume:

148 
$$SED \ (J \ L^{-3}) = \frac{P \ (W)}{Q \ (L^3 / \text{min})} \times t$$

149 where *P* is the discharge power and *Q* is the total flow rate.

150        Effluent compositions were analyzed online using a Fourier transform infra-red (FTIR)  
151        spectrometer (Jasco FT/IR-4200, resolution of 2 cm<sup>-1</sup>) equipped with a 1–16 m variable gas cell  
152        (PIKE Technologies). The effective pathlength of the gas cell used in this study was 5.3 m.  
153        Measurements were carried out after running the plasma system for about 40 minutes, when a steady-  
154        state had been reached. All the signals were obtained by averaging 128 scans. Quantitative analysis  
155        was carried out by comparing the obtained signals with the standard FTIR spectra from Pacific  
156        Northwest National Laboratory (PNNL) database. The removal efficiency of formaldehyde is defined  
157        as:

$$158 \quad \eta_{\text{HCHO}} = \frac{c_{in} - c_{out}}{c_{in}} \times 100\%$$

159        where  $c_{in}$  and  $c_{out}$  are inlet and outlet concentrations of formaldehyde, respectively.

160        The selectivity of carbon dioxide (CO<sub>2</sub>) is defined as follows:

$$161 \quad CO_2 \text{ selectivity} (\%) = \frac{c_{co_2}}{c_{co} + c_{co_2}} \times 100$$

162        where  $c_{co}$  and  $c_{co_2}$  are CO and CO<sub>2</sub> concentrations in the effluent, respectively.

163

## 164        **2.2 Model Description**

165        A Boltzmann equation solver called BOLSIG+ was used to calculate the electron energy  
166        distribution in the plasma together with the energy deposition in various electron-induced collisions  
167        [22][23]. Based on the classical two term approximation, BOLSIG+ provided steady solutions to the  
168        Boltzmann equation in the selected range of the reduced electric field (E/N, ratio of electric field to  
169        the number density of carrier gas molecules, in Td) and gave outputs of the corresponding electron  
170        energy distribution function (EEDF), mean electron energy, reaction rate coefficients and energy

171 fractions of each plasma reaction channel. The reduced electric field was obtained from the  
172 experimental data, while an electron number density of  $10^{19} \text{ m}^{-3}$  was chosen as the initial condition  
173 for the calculation, which was within the same order of magnitude of experimental results ( $10^{18}\text{--}10^{21}$   
174  $\text{m}^{-3}$ ) of air DBDs [24][25]. The cross section data of N<sub>2</sub> and O<sub>2</sub> used in this study was obtained from  
175 Phelps [26] and Lawton [27], while the effect of formaldehyde was excluded due to its low  
176 concentration (57.7 ppm) in the air flow (79% N<sub>2</sub> and 21% O<sub>2</sub>). A list of chosen reactions has been  
177 given in Table S1 (Supporting Information).

178

### 179 **2.3 Catalysts Preparation**

180 A series of Cu-Ce mixed oxides with different Cu/Ce molar ratios (1:3, 1:1 and 3:1) were  
181 prepared using the citric acid method. The desired amount of copper nitrate, ceria nitrate and citric  
182 acid (99.9%, Alfa Aesar) were mixed and then dissolved in deionized water. The molar ratio of citric  
183 acid to metal salts was 1.5. The above solution was stirred at room temperature for 2 h, followed by  
184 drying in a water bath at 80 °C. The obtained samples were heated overnight at 110 °C and then  
185 calcined at 500 °C for 5 h. All the catalysts were sieved in 35-60 meshes for testing. Pure copper  
186 oxide and ceria oxide were prepared using a similar procedure.

187

### 188 **2.4 Catalyst Characterization**

189 N<sub>2</sub> adsorption and desorption experiments were carried out to determine the specific surface area,  
190 pore size distribution and average pore diameter of the catalysts using an Autosorb-1-C instrument  
191 (Quantachrome Instrument Crop). XRD patterns of the catalyst samples were recorded by a Rigaku  
192 D/max 2550PC system with a Cu-K $\alpha$  radiation in the  $2\theta$  range from 10° to 80°. X-ray photoelectron

193 spectroscopy spectra were recorded with a Thermo ESCALAB 250 using Al K $\alpha$  X-ray ( $\text{h}\nu = 1486.6$   
194 eV) at 150 W as a radiation source. Sample charging effect was eliminated by correcting the observed  
195 spectra with the C 1s binding energy (B. E.) value of 284.6 eV. Carbon deposition on the surface of  
196 spent catalysts was evaluated by thermogravimetric analysis (TGA) and differential thermal analysis  
197 (DTA) in an air atmosphere using a Thermal MAX 500 instrument at a heating rate of 10 °C min $^{-1}$   
198 from 20 °C to 900 °C.

199

200 **3. Results and Discussions**

201 **3.1 Catalyst properties**

202 **3.1.1 Structure of Cu-Ce catalysts**

203 The isotherms of nitrogen adsorption/desorption for all the samples are of type IV, which is  
204 associated with capillary condensation in mesopores [28]. Type H3 hysteresis loops are observed  
205 closing at  $P/P_0 = 0.4$  for all the catalysts, which indicate typical open slit-shaped pores with parallel  
206 walls and ink-bottle-shaped pores [29]. Table 1 shows the specific surface area ( $S_{\text{BET}}$ ), total pore  
207 volume and average pore diameter of all the fresh catalysts. A synergy resulting from the interactions  
208 between Cu oxide and Ce oxide can be clearly observed. The specific surface area ( $33.0 - 64.4 \text{ m}^2 \text{ g}^{-1}$ )  
209 of the Cu-Ce catalysts is significantly enhanced compared to that of pure CuO ( $3.6 \text{ m}^2 \text{ g}^{-1}$ ) and  
210 CeO<sub>2</sub> ( $10.3 \text{ m}^2 \text{ g}^{-1}$ ). The highest  $S_{\text{BET}}$  and total pore volume were obtained for the Cu1Ce1 catalyst,  
211 while further increasing of the amount of Cu or Ce resulted in a decrease of the  $S_{\text{BET}}$  and pore volume  
212 of the catalysts.

213

214

Table 1.

Sample	$S_{\text{BET}}$ ( $\text{m}^2 \text{ g}^{-1}$ )	Total pore volume ( $\text{cm}^3 \text{ g}^{-1}$ )	Average pore diameter (nm)	Crystallite size <sup>a</sup> (nm)	Lattice constant <sup>b</sup> ( $\text{\AA}$ )	$\text{Ce}^{3+}$ $/(\text{Ce}^{3+} + \text{Ce}^{4+})$ <sup>c</sup> (%)	$\text{O}_{\text{ads}}$ $/(\text{O}_{\text{ads}} + \text{O}_{\text{lat}})$ <sup>d</sup> (%)
CuO	3.6	0.010	8.4	25.43	-	--	-
Cu3Ce1	33.0	0.044	6.7	5.12	5.4095	19.94	34.05
Cu1Ce1	64.4	0.081	4.4	4.58	5.4097	24.54	38.22
Cu1Ce3	41.7	0.063	6.2	4.77	5.4100	14.55	36.12
CeO <sub>2</sub>	10.3	0.035	7.7	17.44	5.4104	9.78	26.70
Spent Cu1Ce1	60.8	0.078	4.8	4.58	5.4097	23.87	33.02

216     <sup>a</sup> All column data correspond to crystallite size of CeO<sub>2</sub> except for the first one, which corresponds  
 217     to CuO.

218     <sup>b</sup> Calculated from the characteristic peak of CeO<sub>2</sub> (111) crystal face located at  $2\theta = 28.5^\circ$  in the XRD  
 219     patterns.

220     <sup>c</sup> Relative percentage of Ce<sup>3+</sup> on catalyst surface are calculated from XPS data.

221     <sup>d</sup> Relative percentage of surface oxygen species (O<sub>ads</sub>) are calculated from XPS data, while O<sub>lat</sub> is  
 222     lattice oxygen species of Cu-Ce catalysts.

223

224       Fig. 2 presents the XRD patterns of the fresh and spent catalysts. For the CuO catalyst, typical  
 225     diffraction patterns of CuO phase (JCPDS 45-0937) can be clearly seen, while the CeO<sub>2</sub> and all fresh  
 226     Cu-Ce catalysts show a typical cubic fluorite-type oxide structure (JCPDS 34-0394). No obvious  
 227     reflections of a copper oxide phase are found in the Cu1Ce1 and Cu1Ce3 samples, which can be  
 228     attributed to the well dispersed CuO on the surface of CeO<sub>2</sub> [30]. Further increasing of the Cu  
 229     content leads to the formation of bulk CuO particles, since the characteristic peaks of CuO at  $2\theta =$   
 230     35.5° and 38.5° are detected in the Cu3Ce1 catalyst. The diffraction peaks of all the Cu-Ce catalysts  
 231     are broader compared to those of CuO and CeO<sub>2</sub>, while the peak intensities of the Cu-Ce catalysts are  
 232     smaller, indicating the decrease of CeO<sub>2</sub> crystallinity by Cu doping, which is in accordance with the  
 233     calculated crystalline size of CeO<sub>2</sub> (Table 1) using the Scherrer's equation [31]

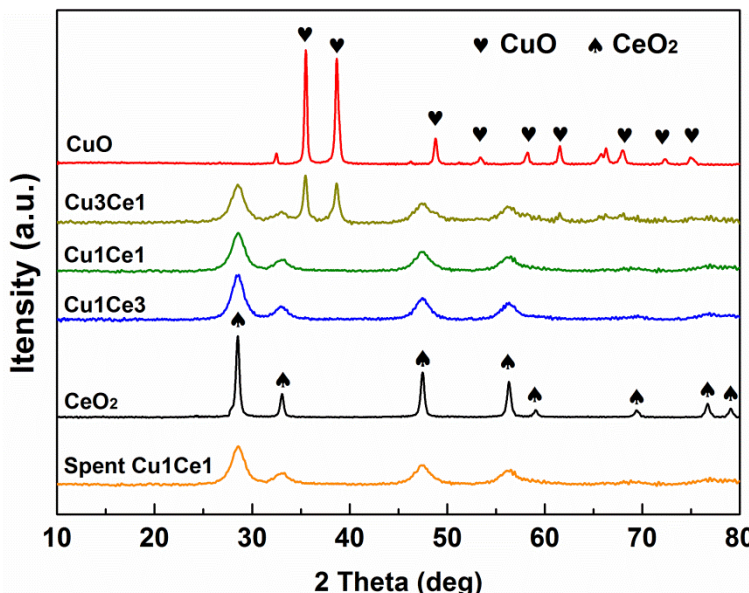
234

$$d = \frac{0.89\lambda}{(\beta - \beta_0)\cos\theta} \quad (2)$$

235 where  $d$  is the average volume diameter of the crystallite,  $\lambda$  is the wavelength of the incident X-rays  
236 from the Cu source,  $\theta$  is the X-ray incidence angle with respect to the sample surface,  $\beta$  is the peak  
237 width at half peak height (in radians) and  $\beta_0$  is the instrumental line broadening.

238 Pure CeO<sub>2</sub> and CuO have a crystallite size of 17.44 nm and 25.43 nm, respectively, but it  
239 decreases significantly to 4.58-5.12 nm in the case of the Cu-Ce catalysts, which is in agreement with  
240 the results of N<sub>2</sub> adsorption-desorption experiments in this study. The XRD patterns of the Cu-Ce  
241 catalysts show a slight shift of about +0.3° for the characteristic peak of CeO<sub>2</sub> (111) crystal face  
242 located at  $2\theta = 28.5^\circ$ . This behavior can be explained by the incorporation of CuO into the CeO<sub>2</sub>  
243 lattice and the partial substitution of Ce cations by Cu cations. Since the radius of Cu<sup>2+</sup> (0.73 Å) is  
244 smaller than that of Ce<sup>4+</sup> (0.97 Å), a contraction of the CeO<sub>2</sub> lattice would occur when Ce<sup>4+</sup> is replaced  
245 by Cu<sup>2+</sup>, as confirmed by the decrease of the lattice constant in Table 1.

246



247

Fig. 2.

248

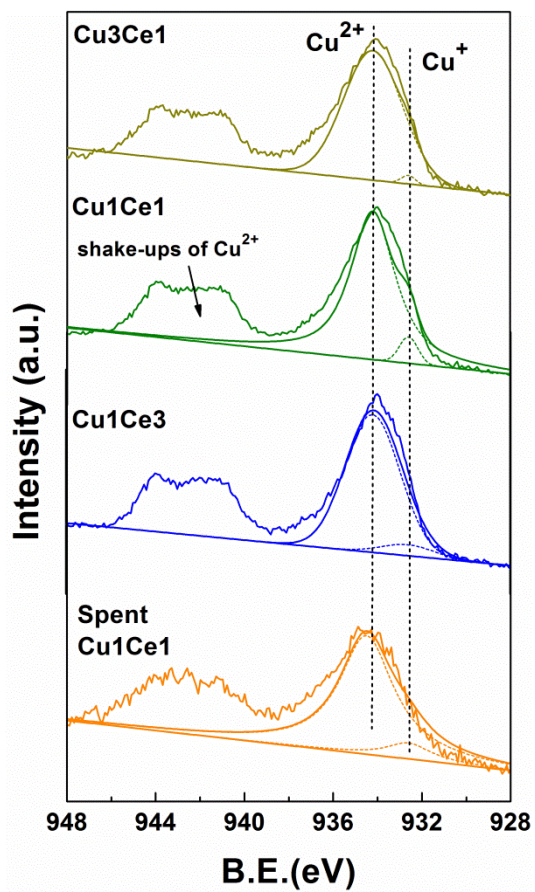
250 **3.1.2 Surface analysis of Cu-Ce catalysts**

251 XPS technique has been used to gain a better insight into the chemical states of all the elements  
252 on the surface of the Cu-Ce catalysts. Fig. 3 shows the XPS spectra of Cu 2p, Ce 3d and O 1s. The  
253 Cu 2p (Fig. 3a) spectra show a main peak of Cu 2p<sub>3/2</sub> at around 934.0 eV, along with the shake-up  
254 peaks at 940-945 eV for all the Cu-Ce catalysts. The presence of the shake-up peaks and their binding  
255 energy demonstrate the existence of Cu<sup>2+</sup> species on the catalyst surface [32]. Deconvolution of Cu  
256 2p<sub>3/2</sub> shows two peaks centered at 934.2 and 932.6 eV, respectively. The former can be identified as  
257 Cu<sup>2+</sup> species, while the latter one belongs to a reduced Cu species (Cu<sup>0</sup> or Cu<sup>+</sup>). It is difficult to  
258 distinguish the exact chemical state of the reduced surface Cu species using XPS since the binding  
259 energy of these two species is very close. However, it is believed that Cu<sup>+</sup> rather than Cu<sup>0</sup> exists as  
260 the main reduced Cu species on the catalyst surface since these catalysts were calcined in air [33].  
261 Cu<sup>+</sup> species can also be formed from the substitution at the interfaces of the oxide phases due to the  
262 similar radius of Cu<sup>+</sup> and Ce<sup>4+</sup> ions [30].

263 The XPS spectra of Ce 3d shows the spin-orbit splitting of Ce 3d<sub>5/2</sub> and Ce 3d<sub>3/2</sub>, labeled as u and  
264 v, respectively (Fig. 3b). The spectra can be divided into ten peaks. The u<sub>2</sub>, u<sub>0</sub>, v<sub>2</sub> and v<sub>0</sub> peaks are  
265 assigned to Ce<sup>3+</sup>, while the rest belong to Ce<sup>4+</sup> [34]. The relative concentration of Ce<sup>3+)/(Ce<sup>3+</sup>+Ce<sup>4+</sup>)</sup>

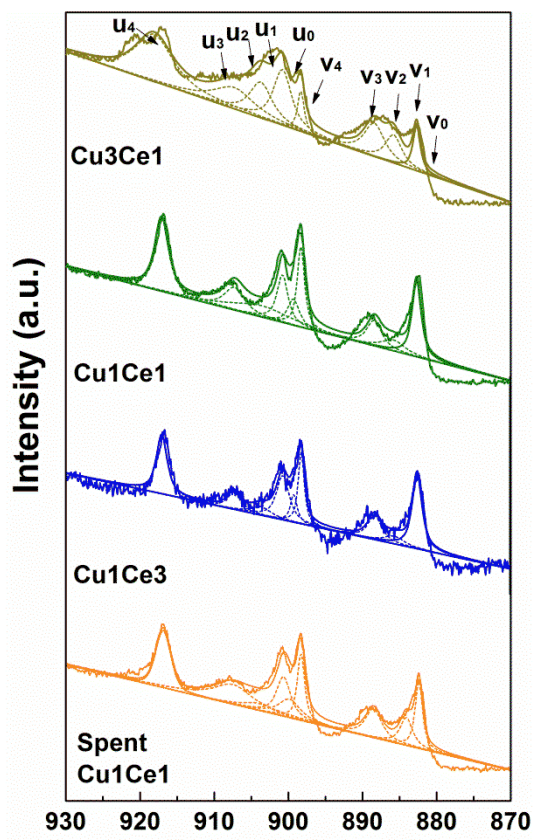
266 ranges from 14.55% to 24.54% for the Cu-Ce catalysts, which suggests that CeO<sub>2</sub> is the main Ce  
267 species on the surface of the Cu-Ce catalysts. The XPS spectra of O 1s are shown in Fig. 3c. Two  
268 components are identified by deconvoluting the main peak at around 531 eV. The peaks at 529.6 eV  
269 are identified as lattice oxygen (O<sup>2-</sup>) (denoted as O<sub>lat</sub>), while those at 531.6 eV are assigned to the  
270 surface adsorbed oxygen (denoted as O<sub>ads</sub>) [35]. The relative concentration of O<sub>ads</sub> ranges from 34.05%  
271 to 38.22% as shown in Table 1, suggesting that lattice oxygen is the most abundant oxygen species  
272 on the surface of the Cu-Ce catalysts.

273



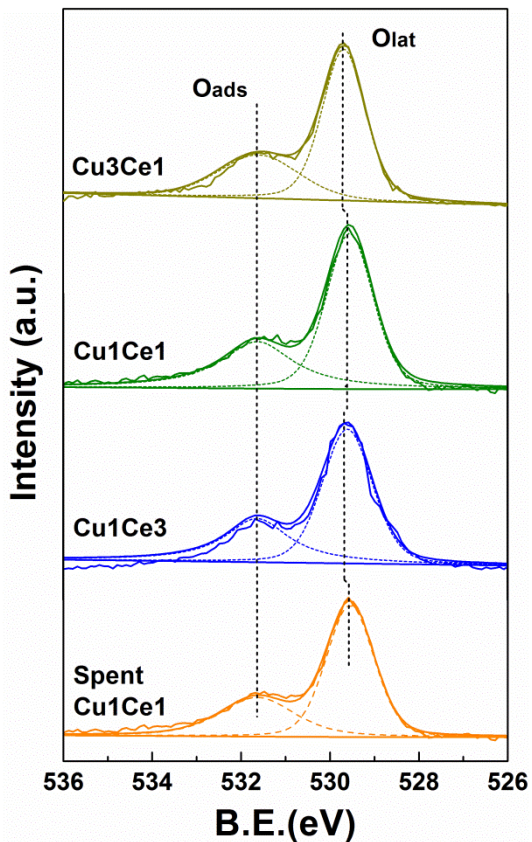
274

(a)



276

(b)



(c)

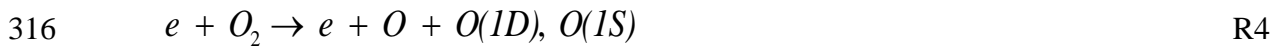
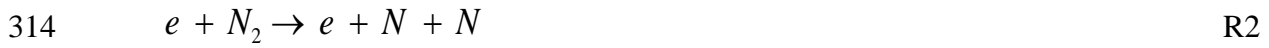
**Fig. 3.**282 **3.2 Plasma-catalytic removal of formaldehyde**

283 Fig. 4 shows the effect of the Cu-Ce catalysts on the removal of formaldehyde as a function of  
 284 SED. The removal of formaldehyde increases with increasing SED regardless of the catalyst used.  
 285 Increasing the SED by raising the applied voltage is expected to effectively enhance the reduced  
 286 electric field (E/N), which changes the electron energy distribution function (EEDF) and enhances  
 287 the mean electron energy. This can be demonstrated by our calculation through solving the Boltzmann  
 288 equation using BOLSIG+. Taking the Cu1Ce1 catalyst for example, increasing the applied voltage  
 289 (peak-to-peak) from 4.86 kV to 6.48 kV significantly increases the SED from  $288 \text{ J L}^{-1}$  to  $486 \text{ J L}^{-1}$ ,

290 which enhances the reduced electric field from 90 Td to 120 Td and consequently increases the mean  
291 electron energy from 2.28 eV to 3.29 eV (shown in Fig. 5a). It is also found that by increasing the  
292 SED, the EEDF shifts with an increase in electron density in the high-energy tail of the distribution  
293 function (Fig. 5b). It is expected that increasing the SED also leads to an increase in the number of  
294 microdischarges per half cycle of the applied voltage. Although it is difficult to quantify the total  
295 number of microdischarges in a DBD system, previous work of Kim et al. has demonstrated through  
296 the use of an intensified charge coupled device (ICCD) camera that increasing the discharge power  
297 enhances the electric field, with the formation of more microdischarges in the plasma [36]. Snoeckx  
298 et al. has simulated the process of plasma-based dry reforming and found the number of micro-  
299 discharge pulses per half cycle has a great influence on the electron density, which in turn affects the  
300 calculated conversion and selectivity of the plasma process [25]. As a result of the combined effects  
301 induced by the increase of the SED, more chemically active species can be generated in the discharge  
302 via electron impacts to drive the plasma chemical reactions.

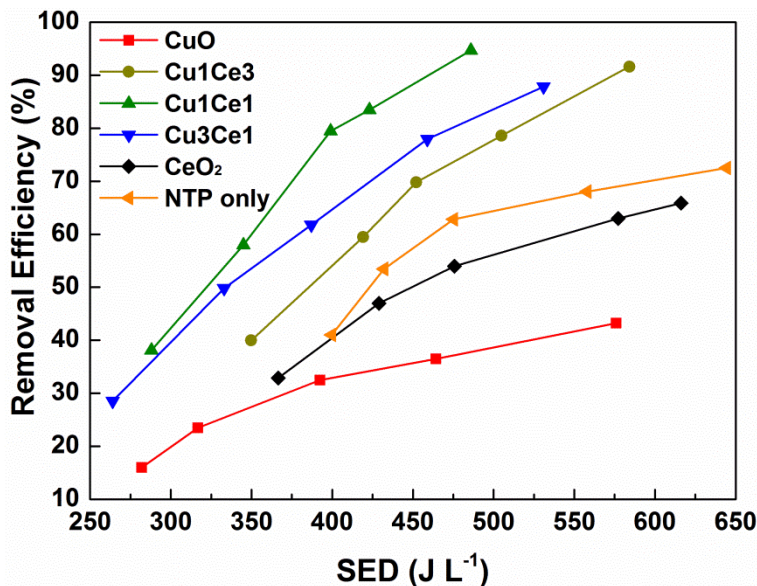
303 To get a better understanding of the initial steps of plasma chemistry, the effect of the reduced  
304 electric field on the fraction of energy transferred to different electron-molecule collision channels  
305 (e.g. elastic, rotational and vibrational excitations, electronic excitations and ionization) has been  
306 investigated (shown in Fig. 5c). In the E/N range of 90 Td to 120 Td, the discharge energy is mainly  
307 consumed by electronic, rotational and vibrational excitations. Electronic excitations become more  
308 important with increasing E/N as its energy fraction increases from 31.0 to 53.6%. Meanwhile, the  
309 discharge power consumed by the rotational and vibrational excitation channels is decreased from  
310 68.6% to 45.6%. Only ~2.5% and ~0.3% of the energy contributes to the minor channels of elastic  
311 and ionization reactions, respectively. Electronic excitation reactions contribute to the generation of

312 N and O radicals and metastable N<sub>2</sub> via R1-R4 [24]:



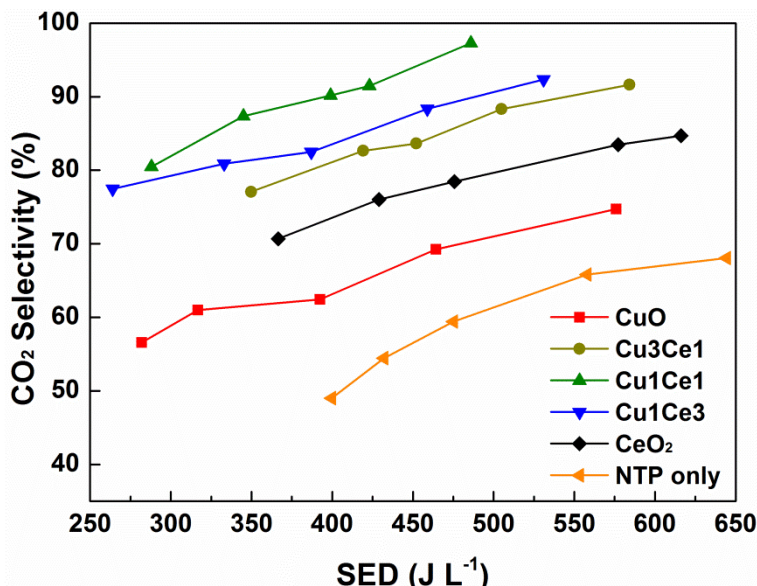
317 where  $N_2(a')$  denotes the sum of N<sub>2</sub> metastable state of  $N_2(a'^1\Sigma)$ ,  $N_2(a^1\Pi)$  and  $N_2(w^1\Delta)$ .

318



319

(a)



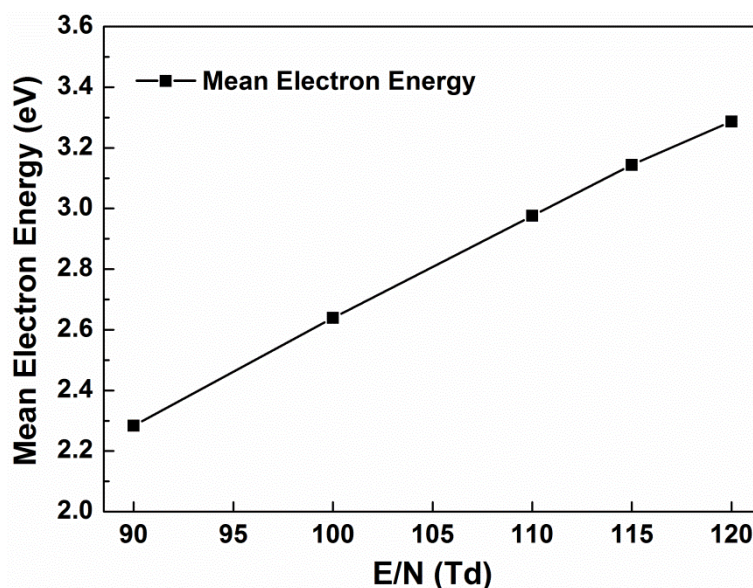
321

322

(b)

323

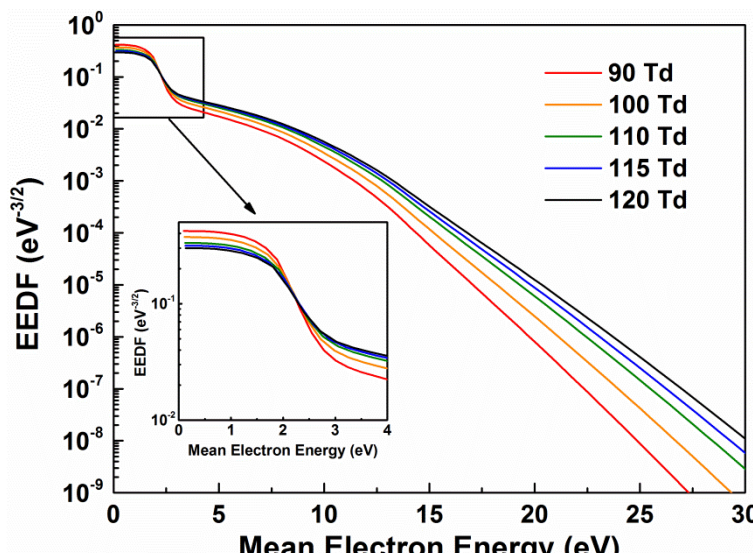
**Fig. 4.**



324

325

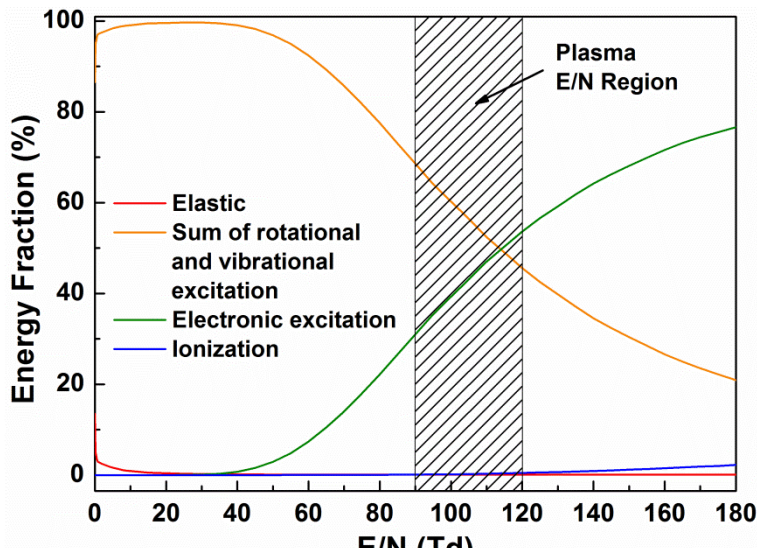
(a)



326

327

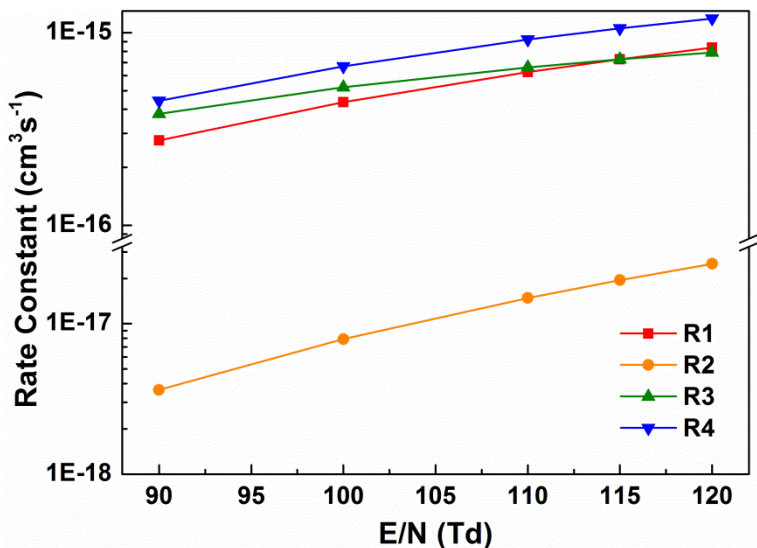
(b)



328

329

(c)



330

331

(d)

332

333

334

As shown in Fig. 5d, the rate coefficient of the reactions R1-R4 is enhanced with the increase in

335

336

337

338

**Fig. 5.**

SED, resulting in the formation of more reactive species. The reactive species with sufficient energy could collide and react with pollutant molecules. The rotational and vibrational excited N<sub>2</sub> and O<sub>2</sub> with insufficient energy are not able to rupture the pollutant molecules, but O<sub>2</sub> species may play a role in the oxidation of the intermediates to CO<sub>2</sub> and H<sub>2</sub>O [24].

339       Compared to the plasma process with no catalyst, the combination of plasma with the Cu-Ce  
340      binary catalysts significantly enhances the removal efficiency of HCHO, while the presence of CuO  
341      or CeO<sub>2</sub> in the DBD reactor has a negative effect on the removal of HCHO. In addition, all the catalyst  
342      samples show an enhanced CO<sub>2</sub> selectivity when combined with the plasma. The highest  
343      formaldehyde removal efficiency (94.7%) and CO<sub>2</sub> selectivity (97.3%) were achieved using the  
344      Cu1Ce1 catalyst at the SED of 486 J L<sup>-1</sup>, as shown in Fig. 4. These results suggest that the interactions  
345      between Cu and Ce species could change the properties of the catalysts, and consequently enhance  
346      the performance of the plasma-catalytic oxidation of formaldehyde. As shown in Table 1, the Cu-Ce  
347      catalysts have a larger specific surface area and pore volume compared to the pure CuO and CeO<sub>2</sub>  
348      samples. It is generally recognized that adsorption is the initial step of heterogeneous catalysis. Higher  
349      adsorption capacity is expected for the Cu-Ce catalysts due to their larger specific surface area which  
350      can provide more adsorption sites and prolong the retention time of formaldehyde in the plasma due  
351      to the diffusion of pollutants within the pores. In a single-stage plasma-catalysis system where the  
352      catalyst is directly in contact with the plasma, reactive species can also be generated in the pores of  
353      the catalysts, thus the probability of reactions between the adsorbed pollutant molecules and reactive  
354      species in the plasma-catalysis system is enhanced [37]. Guaitella et al. found that the adsorption of  
355      C<sub>2</sub>H<sub>2</sub> and active species increased with increasing catalyst porosity, which led to a higher oxidation  
356      of C<sub>2</sub>H<sub>2</sub> in the plasma-catalytic reactions [38]. These results are in good agreement with the findings  
357      of this work as the specific surface areas and pore volumes follow the same order as the removal  
358      efficiency and CO<sub>2</sub> selectivity: Cu1Ce1 > Cu1Ce3 > Cu3Ce1. It is worth noting that high removal  
359      efficiency of 92.9% and CO<sub>2</sub> selectivity of 96.4% are achieved in the plasma-catalytic removal of  
360      HCHO over the Cu1Ce1 catalyst at a SED of 486 J L<sup>-1</sup> after reaction for 5 h, showing the satisfied

361 activity and stability of the Cu1Ce1 catalyst under the experimental conditions. The carbon deposition  
362 (calculated from the TGA curve) on the spent Cu1Ce1 catalyst after 5 h reaction at the SED of 486 J  
363 L<sup>-1</sup> was 0.15%. This weak coke formation could be the reason for the slightly decreased removal  
364 efficiency and CO<sub>2</sub> selectivity. The specific surface area and pore volume of the Cu1Ce1 catalyst was  
365 found to have weakly decreased after the reaction, while the average pore diameter of the catalyst  
366 was slightly increased, as shown in Table 1. These changes could be attributed to the block of micro-  
367 pores on the Cu1Ce1 catalyst by the carbon deposition. The XRD pattern of the spent Cu1Ce1 catalyst  
368 (Fig. 2) shows no significant differences compared to that of the fresh catalyst, indicating the  
369 crystallite structure of the catalyst is not changed by the plasma treatment [39].

370 Previous studies reported the formation of oxygen vacancies on the surface of Cu-Ce catalysts  
371 [40][41]. It is believed that the oxygen vacancies act as adsorption–desorption centers for gas phase  
372 oxygen species, which favors the generation of surface adsorbed oxygen species (O<sub>ads</sub>) on the Cu-Ce  
373 catalysts for the oxidation of formaldehyde [42]. The presence of Ce<sup>3+</sup> on the surface of the Cu-Ce  
374 catalysts confirms the formation of oxygen vacancies. The relative concentration of Ce<sup>3+</sup> in the Cu-  
375 Ce catalysts is found to be much higher than that of pure CeO<sub>2</sub> (9.78%), while the Cu1Ce1 catalyst  
376 shows the highest Ce<sup>3+</sup> concentration, which perfectly matches the reaction performance of the  
377 plasma-catalytic process. Note that the partial substitution of Ce<sup>4+</sup> by Cu<sup>2+</sup> could also lead to the  
378 formation of oxygen vacancies or the reduction of Ce<sup>4+</sup> to Ce<sup>3+</sup> to retain charge balance [43]. The  
379 relative concentration of Ce<sup>3+</sup> in the spent Cu1Ce1 catalyst is slightly less (23.87%) than that of the  
380 fresh catalyst (24.54%), indicating that part of the Ce<sup>3+</sup> are oxidized to Ce<sup>4+</sup> during the plasma-  
381 catalytic process [44].

382 Moreover, the Cu-O and Ce-O chemical bonds can be weakened in the Cu-Ce catalysts due to

383 the electron effect to form more reactive oxygen species and enhance their mobility. As confirmed by  
384 XPS results of O 1s, the relative concentration of the surface adsorbed oxygen species  $O_{ads}$  in the Cu-  
385 Ce samples was higher than that of pure  $CeO_2$ , whilst the highest  $O_{ads}$  concentration of 38.22% was  
386 observed in the fresh Cu1Ce1 catalyst with the best reaction performance. The concentration of  $O_{ads}$   
387 decreased to 33.02% after the plasma reaction of 5 h, which indicates that the surface adsorbed oxygen  
388 species play an important role in the oxidation of formaldehyde on the catalyst surface. The presence  
389 of a higher concentration of  $O_{ads}$  tends to generate more active oxygen species, which could result in  
390 high removal efficiency via surface reactions [41]. A perfect correlation between the reaction  
391 performance and the  $O_{ads}$  concentration for different catalysts is observed in this work.

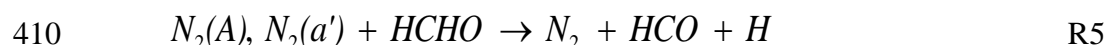
392 The redox properties of the catalysts generated from the interactions between Cu and Ce species  
393 play an important role in the oxidation reactions. Previous studies showed that the redox pairs of  
394  $Cu^{2+}/Cu^+$  and  $Ce^{4+}/Ce^{3+}$  were involved in the electron transfer process from  $Ce^{4+}$  to  $Cu^{2+}$  within the  
395  $Cu^{2+}$ -O- $Ce^{4+}$  connections in the Cu-Ce catalysts. The  $Cu^{2+}$ -O- $Ce^{4+}$  connections could bridge the  
396 oxygen transfer within the structure and reduce the redox potential of the Cu species, which ensures  
397 the improvement of reducibility for both Cu and Ce oxides in the Cu-Ce samples for the plasma-  
398 catalytic oxidation reactions [45].

399

400 **3.3 Reaction mechanisms**

401 The main gaseous products from the plasma-catalytic reactions were CO,  $CO_2$  and  $H_2O$ , while  
402 minor products such as HCOOH were also observed. Ozone was not detected for any of the catalysts,  
403 which might be decomposed due to heating or catalytic decomposition, or consumed in the plasma  
404 oxidation process [46]. In this work, the removal of low concentration formaldehyde in the plasma-

405 catalysis system can be attributed to both plasma gas phase reactions and plasma-assisted surface  
406 reactions on the catalyst surface. The gas phase reactions for the removal of formaldehyde are mainly  
407 induced by plasma generated reactive species such as O, O(1D), OH, N and metastable N<sub>2</sub>, as shown  
408 in R5-R7 [47], while the direct electron-impact collisions only weakly affect the reaction due to the  
409 low concentration of formaldehyde in the carrier gas.

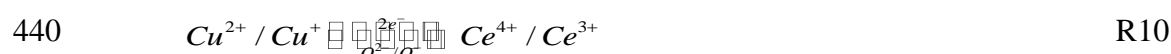


413 As shown in R5-R7, HCO is the main intermediate from the initial steps of HCHO oxidation.  
414 HCO species can be further oxidized by reactive species such as O and O(1D) to form end-products  
415 CO, CO<sub>2</sub> and H<sub>2</sub>O [13]. HCOOH is a common byproduct in plasma processing of HCHO [16].  
416 HCOOH may also be formed from the oxidation of HCHO by O and O(1D) (R8) or the recombination  
417 of HCO with OH (R9):



420 Plasma-assisted surface reactions also contribute to the oxidation of HCHO, while thermal  
421 catalytic activation of HCHO can be ignored due to the relatively low temperature plasma process (<  
422 100 °C) used in this study. In this single-stage plasma catalysis system where the Cu-Ce catalysts  
423 are directly in contact with the discharge, both HCHO and intermediates from the gas phase reactions  
424 can be adsorbed onto the catalyst surfaces. Short-lived active species (e.g. O) generated close to or  
425 on the catalyst surface can participate in the surface reactions. It was reported that the adsorption-  
426 desorption equilibrium can be significantly influenced by plasma [48]. Vibrational excited species

427 generated in plasma may also promote the adsorption of pollutants onto the catalyst surface at low  
 428 temperatures [49]. The enhanced adsorption process increases the collision possibility of pollutants  
 429 and active species, leading to an acceleration of the plasma chemical reactions. The adsorbed species  
 430 could also react with adjacent reactive oxygen species from oxygen vacancies or gas-phase O atoms,  
 431 forming intermediates such as HCO and HCOOH, before finally being oxidized to end-products such  
 432 as CO<sub>2</sub> and H<sub>2</sub>O. Meanwhile, Cu<sup>2+</sup> sites on the catalyst surface could be reduced to Cu<sup>+</sup> and re-  
 433 oxidized to Cu<sup>2+</sup> by the adsorbed oxygen or the lattice oxygen from CeO<sub>2</sub>, which suggests Ce<sup>4+</sup> acts  
 434 as an oxygen source for the oxidation of HCHO [50]. The consumed oxygen species on the catalysts  
 435 can be replenished by capturing oxygen molecules and reactive oxygen species generated in the  
 436 plasma. The fast redox between Ce<sup>4+</sup> and Ce<sup>3+</sup> determines the oxygen storage capacity, which is  
 437 important for the formation of surface oxygen species. Both Cu and Ce are able to shift between  
 438 various oxidation states, while the interaction between Cu and Ce plays a significant role to enclose  
 439 the redox reaction cycle, which determines the catalytic performance [45]:



441 The plausible reaction mechanisms in the plasma-assisted surface oxidation of HCHO are presented  
 442 in Fig. 6:

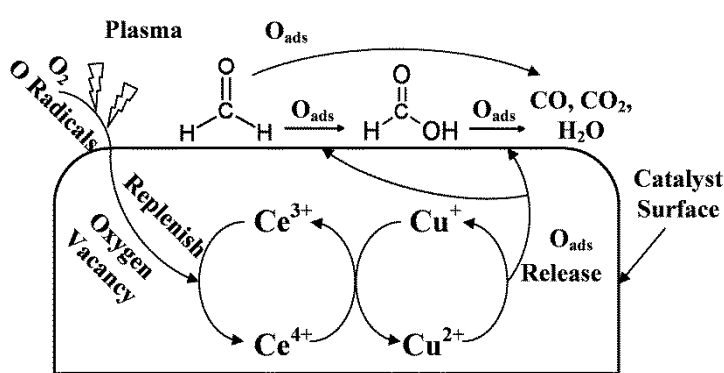


Fig. 6.

446    **4. Conclusions**

447       In this study, the effects of the Cu-Ce catalysts and SED on the plasma-catalytic removal of  
448       formaldehyde have been investigated in terms of the removal efficiency and CO<sub>2</sub> selectivity.  
449       Compared to the plasma process in the absence of a catalyst, the presence of CuO or CeO<sub>2</sub> catalyst in  
450       the plasma decreases the removal efficiency of HCHO, while the combination of plasma with the Cu-  
451       Ce binary metal oxide catalysts significantly enhances the reaction performance regardless of the  
452       SED. This can be ascribed to the interactions between Cu and Ce species over the catalyst surface.  
453       The Cu1Ce1 catalyst (Cu/Ce=1:1) shows the best reaction performance among all the catalysts with  
454       the highest removal efficiency of 94.7% and CO<sub>2</sub> selectivity of 97.3% at the SED of 486 J L<sup>-1</sup>. The  
455       combination of Cu and Ce oxides results in larger specific surface area and characteristic pore volume  
456       and smaller crystalline size, all of which contribute to the plasma-catalytic oxidation of formaldehyde.  
457       The interactions between Cu and Ce oxides also increase the formation of surface adsorbed oxygen  
458       species and facilitate the redox cycles between Cu and Ce species, which plays a key role in the  
459       plasma-induced surface reactions and significantly improves the removal efficiency of formaldehyde.  
460       In this work, the removal of low concentration formaldehyde in the plasma-catalytic process can be  
461       attributed to both plasma gas phase reactions and plasma-assisted surface reactions on the catalyst  
462       surface.

463

464    **Acknowledgements**

465       Support of this work by the Royal Society of the UK (RG120591), the National Natural Science  
466       Foundation of China (No. 51076140 & No. 51206143) and the National Science Fund for  
467       Distinguished Young Scholars (No. 51125025) is gratefully acknowledged.

468

469 **References**

470 [1] H.L. Chen, H.M. Lee, S.H. Chen, M.B. Chang, Ind. Eng. Chem. Res. 47 (2008) 2122-2130.

471 [2] H.H. Kim, Plasma Process. Polymers 1 (2004) 91-110.

472 [3] R. Aerts, X. Tu, W. Van Gaens, J.C. Whitehead, A. Bogaerts, Environ. Sci. Technol. 47 (2013)

473 6478-6485.

474 [4] X. Tu, H. J. Gallon, J. C. Whitehead, J. Phys. D: Appl. Phys. 44 (2011) 482003.

475 [5] R. Aerts, X. Tu, C. De Bie, J. C. Whitehead, A. Bogaerts, Plasma Process. Polymers 9 (2012)

476 994-1000.

477 [6] J. Van Durme, J. Dewulf, C. Leys, H. Van Langenhove, Appl. Catal. B: Environ. 78 (2008) 324-

478 333.

479 [7] E. C. Neyts, A. Bogaerts, J. Phys. D: Appl. Phys. 47 (2014) 224010.

480 [8] J. C. Whitehead, Pure Appl. Chem. 82 (2010) 1329-1336.

481 [9] X. Tu, J.C. Whitehead, Appl. Catal. B: Environ. 125 (2012) 439-448.

482 [10]X. Tu, H. J. Gallon, M. V. Twigg, P. A. Gorry, J. C. Whitehead, J. Phys. D: Appl. Phys. 44 (2011)

483 274007.

484 [11]K. Hensel, Z. Machala, A. Mizuno, 2rd International Workshop on Cold Atmospheric Pressure

485 Plasmas: Sources and Applications, 85-88, Bruges, Belgium, 2005.

486 [12]W.J. Liang, J. Li, J.X. Li, T. Zhu, Y.Q. Jin, J. Hazad. Mater. 175 (2010) 1090-1095.

487 [13]H.X. Ding, A.M. Zhu, F.G. Lu, Y. Xu, J. Zhang, X.F. Yang, J. Phys. D: Appl. Phys. 39 (2006)

488 3603-3608.

- 489 [14]D.Z. Zhao, X.S. Li, C. Shi, H.Y. Fan, A.M. Zhu, Chem. Eng. Sci. 66 (2011) 3922-3929.
- 490 [15]Y. Wan, X. Fan, T. Zhu, Chem. Eng. J. 171 (2011) 314-319.
- 491 [16]X. Fan, T. Zhu, Y. Sun, X. Yan, J. Hazard. Mater. 196 (2011) 380-385.
- 492 [17]H.L. Tidahy, S. Siffert, F. Wyrwalski, J.F. Lamonier, A. Aboukais, Catal. Today 119 (2007) 317-
- 493 320.
- 494 [18]R. Qu, X. Gao, K. Cen, J. Li, Appl. Catal. B: Environ. 142-143 (2013) 290-297.
- 495 [19]S.M. Saqer, D.I. Kondarides, X.E. Verykios, Appl. Catal. B: Environ. 103 (2011) 275-286.
- 496 [20]C. Hu, Chem. Eng. J. 168 (2011) 1185-1192.
- 497 [21]H.J. Li, X.Y. Jiang, X.M. Zheng, Appl. Surface Sci. 280 (2013) 273-281.
- 498 [22]G.J.M. Hagelaar, L.C. Pitchford, Plasma Sources Sci. Technol. 14 (2005) 722-733.
- 499 [23]S. Pancheshnyi, S. Biagi, M.C. Bordage, G.J.M. Hagelaar, W.L. Morgan, A.V. Phelps, L.C.
- 500 Pitchford, Chem. Phys. 398 (2012) 148-153.
- 501 [24]A. Fridman, Plasma chemistry, Cambridge University Press, 2008.
- 502 [25]R. Snoeckx, R. Aerts, X. Tu, A. Bogaerts, J. Phys. Chem. C 117 (2013) 4957-4970.
- 503 [26]A.V. Phelps, L.C. Pitchford, Phys. Rev. A 31 (1985) 2932-2949.
- 504 [27]S.A. Lawton, A.V. Phelps, J. Chem. Phys. 69 (1978) 1055.
- 505 [28]B.C. Lippens, J. De Boer, J. Catal. 4 (1965) 319-323.
- 506 [29]K.S. Sing, Pure Appl. Chem. 57 (1985) 603-619.
- 507 [30]G. Avgouropoulos, T. Ioannides, H. Matralis, Appl. Catal. B: Environ. 56 (2005) 87-93.

- 508 [31]X. Tu, H. J. Gallon, J. C. Whitehead, Catal. Today 211 (2013) 120-125.
- 509 [32]D. Mrabet, A. Abassi, R. Cherizol, T.-O. Do, Appl. Catal. A: General 447 (2012) 60-66.
- 510 [33]W. Liu, M. Flytzani-Stephanopoulos, J. Catal. 153 (1995) 317-332.
- 511 [34]M. Skoda, M. Cabala, I. Matolinova, T. Skala, K. Veltruska, V. Matolin, Vacuum 84 (2009) 8-
- 512 12.
- 513 [35]J.C. Dupin, D. Gonbeau, P. Vinatier, A. Levasseur, Phys. Chem. Chem. Phys. 2 (2000) 1319-
- 514 1324.
- 515 [36]H.H. Kim, A. Ogata, Eur. Phys. J. Appl. Phys. 55 (2011) 13806.
- 516 [37]F. Holzer, Appl. Catal. B: Environ. 38 (2002) 163-181.
- 517 [38]O. Guaitella, F. Thevenet, E. Puzenat, C. Guillard, A. Rousseau, Appl. Catal. B: Environ. 80
- 518 (2008) 296-305.
- 519 [39]X. Tang, K. Li, H. Yi, P. Ning, Y. Xiang, J. Wang, C. Wang, J. Phys. Chem. C 116 (2012)
- 520 10017-10028.
- 521 [40]G. Marbán, A.B. Fuertes, Appl. Catal. B: Environ. 57 (2005) 43-53.
- 522 [41]G. Zhou, H. Lan, T. Gao, H. Xie, Chem. Eng. J. 246 (2014) 53-63.
- 523 [42]M. Roxana Morales, F.N. Agueero, L.E. Cadus, Catal. Lett. 143 (2013) 1003-1011.
- 524 [43]A. Martinezarias, D. Gamarra, M. Fernandezgarcia, X. Wang, J. Hanson, J. Rodriguez, J. Catal.
- 525 240 (2006) 1-7.
- 526 [44]W. Shan, M. Fleys, F. Lapicque, D. Swierczynski, A. Kiennemann, Y. Simon, P.-M. Marquaire,
- 527 Appl. Catal. A: General 311 (2006) 24-33.

- 528 [45]U. Menon, H. Poelman, V. Bliznuk, V.V. Galvita, D. Poelman, G.B. Marin, J. Catal. 295 (2012)  
529 91-103.
- 530 [46]F. Holzer, F.D. Kopinke, U. Roland, Plasma Chem. Plasma Process. 25 (2005) 595-611.
- 531 [47]N. Blin-Simiand, S. Pasquier, F. Jorand, C. Postel, J.R. Vacher, J. Phys. D: Appl. Phys. 42  
532 (2009) 122003.
- 533 [48]N. Blin-Simiand, P. Tardiveau, A. Risacher, F. Jorand, S. Pasquier, Plasma Process. Polymers 2  
534 (2005) 256-262.
- 535 [49]T. Nozaki, H. Tsukijihara, W. Fukui, K. Okazaki, Energy & Fuels 21 (2007) 2525-2530.
- 536 [50]C. He, Y. Yu, C. Chen, L. Yue, N. Qiao, Q. Shen, J. Chen, Z. Hao, RSC Advances 3 (2013) 19639.
- 537
- 538
- 539
- 540
- 541
- 542 **Figure captions**
- 543 Fig. 1. Schematic diagram of the experimental setup.
- 544 Fig. 2. XRD patterns of fresh and spent catalysts.
- 545 Fig. 3. XPS spectra of fresh and spent Cu-Ce binary catalysts (a) Cu 2p; (b) Ce 3d; (c) O 1s.
- 546 Fig. 4. Effect of different catalysts on (a) removal efficiency of formaldehyde; (b) CO<sub>2</sub> selectivity as

547 a function of SED.

548 Fig. 5. (a) Calculated mean electron energy; (b) EEDF; (c) energy fraction consumed in different

549 electron impact reactions; (d) rate constants of reactions for the formation of N and O radicals in the

550 plasma-catalysis system over the Cu1Ce1 catalyst (E/N: 90 - 120 Td; SED: 288-486 J L<sup>-1</sup>).

551 Fig. 6. Plausible reaction mechanisms on catalyst surface.

552

553 **Table Captions**

554 Table. 1. Physicochemical characteristics of the catalysts.

555

556

557